Pharm Res (2015) 32:3899–3915
DOI 10.1007/s11095-015-1750-y

RESEARCH PAPER

Elucidation of Molecular Mechanisms Behind the Self-Assembly Behavior of Chitosan Amphiphilic Derivatives Through Experiment and Molecular Modeling

Mohammad Mahmoudzadeh[1,2] • Afshin Fassihi[1,3] • Farid Dorkoosh[4] • Reyhaneh Heshmatnejad[5] • Karim Mahnam[6] • Hassan Sabzyan[7] • Amir Sadeghi[1]

Received: 13 January 2015 / Accepted: 6 July 2015 / Published online: 12 August 2015

ABSTRACT

Purpose Chitosan-based polymeric micelles (CBPMs) are considered as promising carriers for delivery of anticancer drugs, imaging agents and genes. To optimize the physicochemical, pharmaceutical and biological properties of CBPMs, the molecular mechanisms behind the self-assembly behavior of chitosan (CHI) amphiphilic derivatives are elucidated.

Methods This study has two stages. In the experimental stage, dexamethasone (DEX) as a hydrophobic group is grafted to CHI in three degrees of substitution in order to obtain CHI derivatives with different degrees of hydrophobicity. These new CHI amphiphilic derivatives (CHI_DEXs) form micelles in water where their critical aggregation concentration (CAC), size and zeta potential are measured. Through comparing the results of these measurements, the change of self-assembly behavior of CHI_DEXs in response to increasing their hydrophobicity is evaluated. Correlating this evaluation with the results of the 13 MD simulations conducted on CHI_DEXs in atomistic molecular dynamics (MD) simulation stage, reveals the molecular mechanisms behind the self-assembly behavior of CHI_DEXs.

Results Our evaluation of the experimental results reveals that increasing hydrophobicity of a CHI amphiphilic derivative would not necessarily cause it to form micelles with lower CAC value, smaller size and lower zeta potential. The MD simulations reveal that there exists a balance between intra- and inter-chain interactions which is responsible for the self-assembly behavior of CHI amphiphilic derivatives.

Conclusion An increase in DS of the hydrophobic group triggers a cascade of molecular events that shifts the balance between intra- and inter-chain interactions leading to changes in the CAC, size and zeta potential of the CBPMs.

KEY WORDS chitosan · molecular dynamics simulation · molecular mechanisms · polymeric micelles · self-assembly

ABBREVIATIONS

^{1}HNMR	^{1}H nuclear magnetic resonance
CAC	Critical aggregation concentration
CBPMs	Chitosan-based polymeric micelles
CHI	Chitosan
DCC	Dicyclohexyl carbodiimide

Electronic supplementary material The online version of this article (doi:10.1007/s11095-015-1750-y) contains supplementary material, which is available to authorized users.

✉ Afshin Fassihi
fassihi@pharm.mui.ac.ir

✉ Amir Sadeghi
sadeghi_am5@yahoo.com

[1] Department of Medicinal Chemistry, Faculty of Pharmacy, Isfahan University of Medical Sciences, Isfahan, Iran

[2] Department of Pharmaceutics, Faculty of pharmacy, Isfahan University of Medical Sciences, Isfahan, Iran

[3] Isfahan Pharmaceutical Sciences Research Center, Isfahan, Iran

[4] Department of Pharmaceutics, Faculty of Pharmacy, Tehran University of Medical Sciences, Tehran, Iran

[5] Department of Chemical Engineering, Faculty of Engineering, University of Isfahan, Isfahan, Iran

[6] Biology Department, Faculty of Sciences, Shahrekord University, Shahrekord, Iran

[7] Department of Chemistry, University of Isfahan, Isfahan, Iran

DEX	Dexamethasone
DMAP	4-dimethylaminopyridine
DS	Degree of substitution
FT-IR	Fourier transform infrared
GPUs	Graphics processing units
Hbonds	Hydrogen bonds
HHB	Hydrophobicity-hydrophilicity balance
MD	Molecular dynamics
MM-GBSA	Molecular mechanics with generalized Born and surface area solvation
NHS	N-hydroxy succinimide
nmode	Normal mode
NPT	Isothermal-isobaric ensemble
ns	Nanosecond
NVT	Canonical ensemble
OW	Water oxygens
PME	Particle mesh Ewald
ps	Picosecond
RDF	Radial distribution function
RMSD	Root mean square deviation
SASA	Solvent accessible surface area
SUC	Succinic anhydride
TEM	Transmission electron microscope

INTRODUCTION

The CBPMs widespread application in delivery of therapeutic and diagnostic agents (1–3) is based on their adjustable Physicochemical, pharmaceutical and biological properties (4). If molecular mechanisms behind the self-assembly behavior of CHI amphiphilic derivatives are elucidated, these properties could be adjusted through modification of the ratio and chemical structure of the three main constituents of CHI amphiphilic derivatives that are: CHI as the backbone, the hydrophilic group and the hydrophobic group. The hydrophilic and the hydrophobic groups are covalently grafted to CHI which is a biodegradable and biocompatible natural polysaccharide with the repeating units of D-glucosamine and N-acetyl-D-glucosamine in different ratios (5).

In this study, at first the self-assembly behavior of CHI amphiphilic derivatives is evaluated and then molecular mechanisms behind it would be elucidated. Evaluation of self-assembly behavior of these derivatives is a complex task. To reduce the complexity of this task, we exclude the effect of hydrophilic group in the self-assembly behavior of CHI amphiphilic derivatives. Therefore, in this study the change of self-assembly behavior of CHI amphiphilic derivatives in response to increasing their hydrophobicity is evaluated. To exclude the necessity of hydrophilic modification of CHI for the synthesis of CHI amphiphilic derivatives with the capability of micelle formation, in the experimental stage oligoCHI is used as the backbone. Since oligoCHI is water-soluble, grafting a hydrophobic group in a proper DS to CHI should suffice to provide CHI amphiphilic derivatives with the capability of micelle formation in aqueous solutions (6,7). Therefore, DEX as a hydrophobic group is grafted to CHI in three DSs of 6, 11.5 and 16.5% to obtain CHI_DEXs with different degrees of hydrophobicity as models of CHI amphiphilic derivatives. Due to difference in hydrophobicity, the self-assembly behavior of the three CHI_DEXs would be different from each other which would lead to the formation of micelles with different size, CAC, and zeta potential. Evaluation of the self-assembly behavior of the CHI_DEXs is performed through measuring and comparing CAC, size and zeta potential of the formed micelles.

In the MD simulations stage, 13 atomistic MD simulations are conducted on CHI_DEXs. Through these simulations, single-chains geometry, self-assembly tendency of CHI_DEXs, the balance of intra- and inter-chain interactions, self-assembly energy analysis, local behavior of water molecules around the polymeric chains and Hbonds role in the self-assembly process of CHI_DEXs are evaluated. Correlating simulations results with the evaluations of the experimental stage would lead to the elucidation of molecular mechanisms behind the self-assembly behavior of CHI_DEXs. To the best of our knowledge, this is the first study in which both the experiment and MD simulations are applied for the elucidation of molecular mechanisms behind the self-assembly behavior of CHI amphiphilic derivatives.

METHODS

Experimental Methods

Materials

CHI (MW of 10 kDa, deacetylation degree of 90%) is purchased from Yuhuan Marine Biochemistry, Zhejiang, China. DEX, succinic anhydride (SUC) and 4-dimethylaminopyridine (DMAP) are purchased from Merck. N-hydroxy succinimide (NHS), Dicyclohexyl carbodiimide (DCC), Dialysis tube (MW cut off 2 kDa), Syringe filter (0.22 μm) and all the solvents are purchased from Sigma-Aldrich.

Synthesis of CHI_DEXs

As shown in Fig. 1, the first stage of the synthesis of the CHI_DEXs is the synthesis of dexamethasone-succinate (DEX_SUC). The SUC would serve as a spacer which provides a carboxylic group for DEX to form an amide bond with the amino groups of CHI. The esterification reaction between DEX and SUC is carried out according to the procedure described by Mcleod *et al.* (8) with minor modifications. The

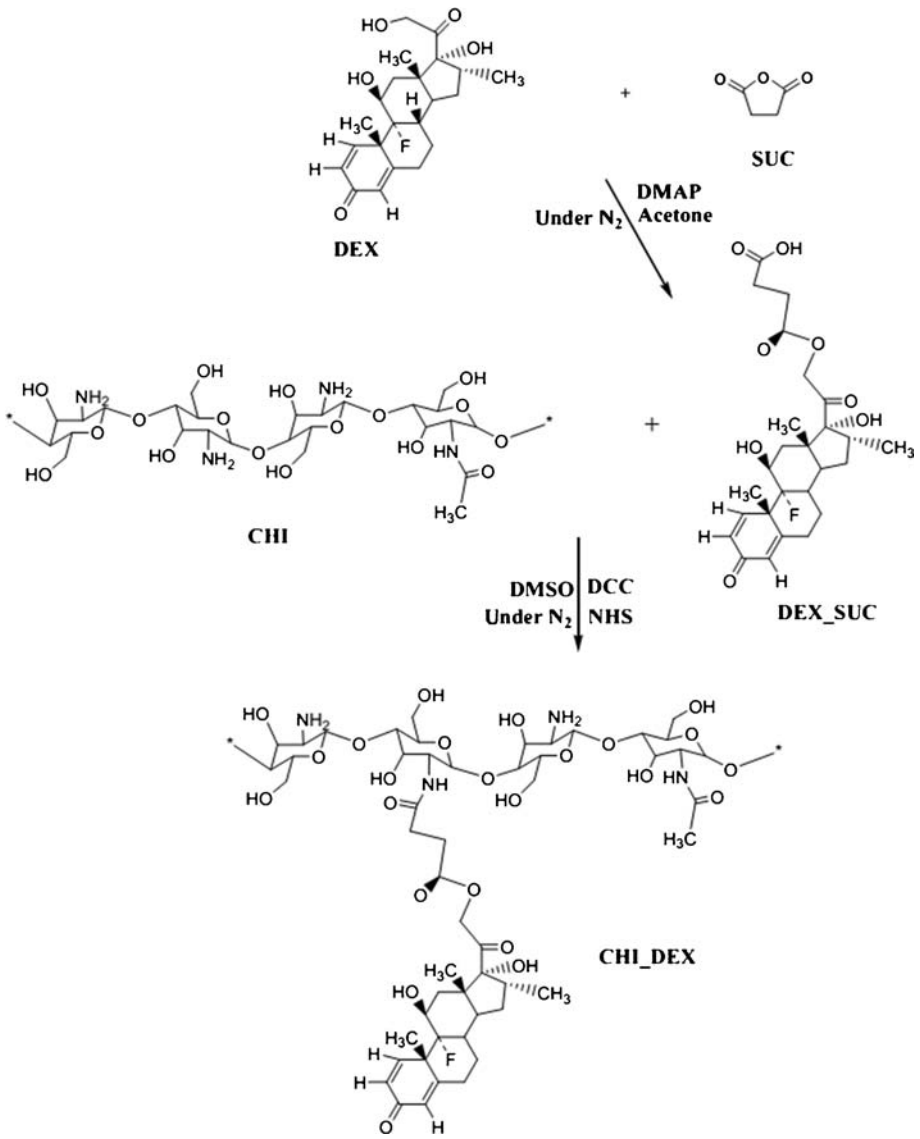

Fig. 1 Synthesis procedure of CHI_DEXs.

reaction solution is prepared by dissolving 0.01 mol of DEX, 0.012 mol of SUC and 0.012 mol of DMAP in anhydrous acetone. This solution is stirred for 72 h under nitrogen in an anhydrous condition. Next, the acetone is removed and an off-white powder is gained. Then, this powder is dissolved in ethanol and water is added gradually to the solution. This solution is kept at 4°C for 24 h until white crystals are precipitated. These crystals are separated and dried under vacuum.

In the second stage, the CHI_DEXs are synthesized by the amide reaction of the carboxyl group of DEX-SUC with the amino groups of CHI (Fig. 1). The reaction between DEX_SUC and CHI is carried out in four molar ratios of DEX-SUC to CHI as follow: 0.06:1, 0.125:1, 0.25:1 and 0.5:1. According to the ^{1}HNMR spectra, the first three molar ratios lead to DSs of 6, 11.5 and 16.5% for DEX on CHI, respectively that we name these three derivatives CHI_DEX6%, CHI_DEX11.5% and CHI_DEX16.5%. The 0.5:1 molar ratio results in the synthesis of a CHI _DEX derivative that is not soluble in water due to high DS of DEX. Here, no analysis is conducted on this CHI derivative. The synthesis procedure for all molar ratios is the same, and thus for brevity, it is described here for the CHI_DEX11.5% only. DEX_SUC (0.3 mmol), NHS (0.9 mmol) and DCC (0.9 mmol) are dissolved in anhydrous dimethylsulfoxide (DMSO). This solution is stirred at room temperature under nitrogen atmosphere for 5 h and then added to the CHI (2.4 mmol) aqueous solution and the reaction is left to proceed for 38 h under nitrogen gas. This mixture is then centrifuged and filtered so that dicyclohexylurea formed as a by-product of the reaction is separated. The final product is precipitated by pouring the filtrate into a large volume of acetone. This precipitate is centrifuged and washed repeatedly by the acetone/methanol mixture. For

further purification, the precipitate is dissolved in deionized water and dialyzed against methanol for 48 h, then against water for 24 h using a dialysis tube (MW cut off 2 kDa) and finally is freeze-dried. The FT-IR and ^{1}HNMR spectra confirming successful synthesis of DEX_SUC and CHI_DEXs are recorded on a FT-IR spectrometer (Jasco FT-IR-6300, Japan) and Bruker 500 MHz spectrometer (Germany), respectively.

Experimental Characterization of Micelles

CHI_DEXs form micelles in water. In order to prepare CHI_DEXs micellar solutions, first, CHI_DEXs are dissolved in deionized water with the concentration of 1 mg/mL and next, the solutions are probe-sonicated in an ice bath at 50 W for 2 min (pulse on 2 s, pulse off 2 s). These micellar solutions are used for the observation of morphology of micelles through transmission electron microscope (TEM) and evaluation of the self-assembly behavior of CHI_DEXs through measuring CAC, size and zeta potential of micelles.

To observe the morphology of the micelles, one drop of sample solution is placed onto a copper grid coated with carbon and air dried for 15 min. The morphology of micelles is observed by TEM (Ziess, Germany) operating at an accelerating voltage of 60 kV.

To measure the CAC of CHI_DEXs, fluorescence spectroscopy is performed using pyrene as a fluorescence probe through the procedure described by Yinsong *et al.* (9) with a minor modification. First, the pyrene solution in acetone is added into the test tubes and the acetone is removed under nitrogen purge. Next, the CHI_DEXs micellar solutions in various concentrations ranging from 6×10^{-5} to 1 mg/mL, are added to each test tube adjusting the final concentration of pyrene to 6×10^{-7} M. Then, the mixtures are sonicated in an ultrasonic bath for 30 min and left for 1 h at room temperature. Finally, the pyrene emission spectra is obtained using a fluorescence spectrophotometer (Jasco FP 750, Japan) at the excitation wavelength of 336 nm and the emission range of 350–450 nm.

The size and zeta potential of the micelles are measured by dynamic light scattering (DLS) through a Zetasizer (Malvern Instruments Ltd., UK).

Computational Methods

To elucidate the molecular mechanisms behind the self-assembly behavior of CHI_DEXs, 13 systems are constructed for simulations (Table I). Using Accelrys Discovery Studio Visualizer software, the initial structures of the CHI_DEXs are constructed in one-third of their actual size to reduce the geometrical complexities and computational cost of the simulations. This simplification makes the interpretation of the simulation results more feasible as well. Regarding actual MW of CHI (10 kDa) used in our experiments and the MW of one CHI monomer, one CHI chain is composed of approximately 51 monomers. However, in the MD simulations 17 monomers are considered for one CHI chain. Since we intend to simulate the polymeric chains in one-third of their actual size, one, two and three DEX residues are considered for CHI_DEX6%, CHI_DEX11.5% and CHI_DEX16.5%, respectively. However, in experiment, there are approximately 3, 6 and 9 DEX residues grafted to each CHI chain of CHI_DEX6%, CHI_DEX11.5% and CHI_DEX16.5%, respectively.

Considering the pK_a of CHI (10), half of the amino groups of the backbone are assumed to be protonated. Two out of the 17 monomers of CHI are considered as acetylated in order to model the degree of deacetylation of CHI. To carry out a systematic evaluation of the self-assembly behavior of CHI_DEXs, in addition to CHI_DEXs, we conducted MD simulations on the CHI chains.

The MD simulations of the systems are performed through the AMBER 12.0 package (11). Atom types and force field parameters are generated using the Antechamber program (12) and general amber force field (GAFF) (13). Partial charge of atoms is obtained by means of AM1-BCC method (14,15).

Before solvating each system, a short minimization in vacuum is performed. Then, the Cl^- ions are added to neutralize the charge of the systems. The solvation of the systems is performed using an octahedral box of TIP3P water keeping a 20 Å minimum distance between each face of the box and the solute. The minimization procedure for the solvated systems has two stages: first, the chains are restrained and just geometries of the water molecules and ions are minimized; second, the entire system is minimized. Following the minimization stages, the systems are heated up to 300 K during 20 picoseconds (ps) at canonical ensemble (NVT) using periodic boundary conditions, time step of 2 femtosecond, the Langevin thermostat (16) and 10 Å cutoff for nonbonded interactions. The particle mesh Ewald (PME) approach is applied to calculate long-range electrostatic effects (17) and the SHAKE algorithm is used to constrain all of the bonds that involve the hydrogen atoms (18). Following heating, a 50 ps MD in NPT (isothermal-isobaric ensemble) condition is carried out to relax the density of water. Then, a production phase of 50 ns begins using graphics processing units (GPUs) accelerated Amber codes (19) on a single GTX780 GPUs. The coordinate of atoms are saved every 20 ps in trajectory files and analyzed using AmberTools13 package (11). The VMD software is used to visualize the trajectories and to render the graphical representations of the system (20). Naccess package is used to calculate the solvent accessible surface area (SASA) (21).

It is worth mentioning that if the investigation of the whole phenomenon of micelle formation was intended in this study, instead of atomistic MD simulation, methods such as coarse grain and dissipative particle dynamics simulations which provide the opportunity of much longer simulation times than the atomistic MD simulation (22,23) should have been

Table I Details of the Simulated Systems

System name	System abbreviated name	Number of atoms[a]	Simulation time (ns)
CHI_single-chain	CHI _1	62,939	50
CHI _DEX6%_single-chain	CD6%_1	63,106	50
CHI _ DEX 11.5%_single-chain	CD11.5%_1	44,482	50
CHI _ DEX 16.5%_single-chain	CD16.5%_1	48,811	50
CHI _single-chain_pyrene	CHI _1_p	27,697	30
CHI _ DEX 6%_single-chain _pyrene	CD6%_1_p	18,039	30
CHI _ DEX11.5%_single-chain _pyrene	CD11.5%_1_p	19,953	30
CHI _ DEX16.5%_single-chain _pyrene	CD16.5%_1_p	32,895	30
CHI _hexamer	CHI _6	121,992	50
CHI _ DEX6%_hexamer	CD6%_6	77,724	50
CHI _ DEX11.5%_hexamer	CD11.5%_6	87,822	50
CHI _ DEX16.5%_hexamer	CD16.5%_6	120,474	50
CHI _ DEX11.5%_thirty-chains	CD11.5%_30	885,417	50

[a] Contains the number of polymer, ions and water atoms

applied. Since elucidation of the molecular mechanisms behind the self-assembly behavior of CHI_DEXs needs atomistic details of intra- and inter-chain interactions, the atomistic MD simulation is applied in this study.

The atomistic MD simulations begin by 50 ns simulation of the single-chain systems (CHI _1, CD6%_1, and CD11.5% _1, CD16.5% _1) to equilibrate their geometry in water. To assure equilibrium, root mean square deviation (RMSD) analysis is conducted on the 50 ns trajectories of the single-chain systems. The last 10 ns of these trajectories is used for clustering analysis (24) in order to determine the dominant conformation of the single-chains. These dominant conformations are used for constructing the initial configuration of hexamer systems which are used for the evaluation of self-assembly tendency of CHI_DEXs. To evaluate the self-assembly tendency of CHI_DEXs, 50 ns MD simulations are performed on the hexamer systems (CHI _6, CD6%_6, CD11.5%_6, CD16.5%_6). To construct the initial configuration of each hexamer system, the dominant conformation of its single-chain is copied five times, and then the total of six chains are put beside each other in a manner where the chains have the most contact surface. With respect to the water content of the simulation box and molecular weight of the derivatives, hexamer systems simulate a concentration higher than the CAC value of CHI_DEXs. In order to determine the necessity of hydrophobic modification of CHI for the formation of effective hydrophobic interactions, we evaluate the interactions of pyrene as a hydrophobic probe with the dominant conformation of the single-chains using docking and MD simulation. The initial configurations of single-chain_pyrene complexes are constructed by Autodock package (25). These complexes (CHI _1_p, CD6%_1_p, CD11.5%_1_p, CD16.5%_1_p) are simulated for 30 ns in the presence of TIP3P explicit water.

In our last MD simulation, the balance between intra- and inter-chain interactions is evaluated in a greater scale. Therefore, a 50 ns MD simulation is conducted on a system composed of five copies of initial configuration of CD11.5%_6 (CD11.5%_30).

The calculation of the enthalpy of chains self-assembly is based on the molecular mechanics with generalized Born and surface area solvation (MM-GBSA) approach (26). To determine the contributing energies in the enthalpy of the self-assembly process, the MM-GBSA analysis is conducted on the last 24 snapshots of the CD16.5%_6 trajectory applying the single-trajectory method. Due to high computational cost, we performed energy analysis only on two (out of six) chains of the CD16.5%_6. In each computation, one of these chains is considered as the ligand and the other five as the receptor. The ΔG_{bind} is calculated according to the following equations (26):

$$\Delta G_{self-assembly} = \Delta G_{bind} = G(complex) - [G(receptor) + G(ligand)] \quad (1)$$

$$G(molecule) = E_{gas} + G_{sol} - TS \quad (2)$$

$$E_{gas} = E_{int} + E_{ele} + E_{vdw} \quad (3)$$

$$G_{sol} = G_{sol\_polar} + G_{sol\_nonpolar} \quad (4)$$

$$G_{sol\_nonpolar} = \gamma SASA \quad (5)$$

where E_{gas} is the gas-phase energy, E_{int} is the internal energy, E_{ele} and E_{vdw} are the electrostatic and van der Waals energies, respectively. The G_{sol} is the solvation free energy and can be decomposed into polar and nonpolar contributions. The G_{sol_polar} is the polar solvation free energy calculated through

solving generalized-Born (GB) equation (26,27). The $G_{sol\_nonpolar}$ is the nonpolar solavation free energy and is estimated by the use of the SASA and the surface tension constant (γ) with the value of 0.0072 kcal/mol Å^2 (28). In this study, ΔG_{bind} is used as an index for the self-assembly tendency of chains, named here as $\Delta G_{self\text{-}assembly}$.

To obtain $\Delta G_{self\text{-}assembly}$, we calculated the contribution of the entropy changes ($-T\Delta S$) to chains self-assembly through normal mode (nmode) analysis (29) on the last 24 snapshots taken from the equilibrated trajectories of the MD simulation using the nmode program in AmberTools13 (11). For the nmode calculations, the structures are fully minimized for 10,000 steps until the root-mean square of the elements of the gradient vector becomes less than 0.001 kcal/mol Å^2.

RESULTS AND DISCUSSION

Experimental Results

^{1}H Nuclear Magnetic Resonance (^{1}HNMR) and Fourier Transform Infrared (FT-IR) Spectroscopy Analyses

As shown in Fig. 1, the first stage in the synthesis of the CHI_DEXs is the synthesis of DEX_SUC. The successful synthesis of DEX_SUC is confirmed by ^{1}HNMR analysis. The broad peak at 12.28 ppm which is denoted by b in Fig. 2a is assigned to the hydrogen of carboxylic group of DEX_SUC. The hydrogens of the A ring of DEX observed at 7.29, 6.23 and 6.01 ppm in the spectrum are marked by e, f, and g, respectively. The peaks at 1.49, 0.88 and 0.78 ppm marked by the letters d, c and a, respectively, belong to the hydrogens of methyl groups of DEX. The peaks characterized by the letters m and n, belong to the hydrogen of hydroxyl groups of the C and D rings of DEX, respectively. The peaks at 2.5 and 3.3 ppm in ^{1}HNMR spectrum of DEX_SUC represented by x and z belong to the residual DMSO and water of DMSO-d6.

The second stage in the synthesis of the CHI_DEXs is the formation of amide bond between the carboxylic group of DEX_SUC and amino groups of CHI (Fig. 1). Following this chemical reaction, the peak corresponding to the hydrogen of carboxylic group of DEX_SUC disappears from the ^{1}HNMR spectrum of CHI_DEXs and other peaks corresponding to the hydrogens of DEX_SUC appear next to CHI peaks which indicate the successful synthesis of CHI_DEXs (Fig. 2b). The peak at 4.8 ppm represented by p, belongs to the residual water in D_2O.

The DS of DEX in the CHI_DEXs is calculated based on the integral ratio of the signals a and c corresponding to the hydrogens of the two methyl groups of DEX to signal k corresponding to the ($-C\underline{H}$-NH_2) of CHI.

The successful synthesis of DEX_SUC and CHI_DEXs is confirmed by FT-IR analysis as well. The appearance of the peak at 1716 cm^{-1} in DEX-SUC FT-IR spectrum (Fig. 2c) corresponding to the carbonyl group of esteric bond between DEX and SUC indicates the synthesis of DEX-SUC. Chemical reaction between DEX and SUC would lead to the formation of a carboxylic group (Fig. 1). Two peaks corresponding to this newly formed carboxylic acid group appear in the FT-IR spectrum of DEX_SUC (Fig. 2c) one at 1737 cm^{-1} corresponding to the carboxylic carbonyl group and one at 3229 cm^{-1} corresponding to carboxylic hydroxyl group. Characteristic peaks in the FT-IR spectrum of DEX appear in the FT-IR spectrum of DEX-SUC as well which some of them are as follows: the peak at 1621 cm^{-1} belongs to the stretch C=C bond of the A ring of DEX which appears in 1618 cm^{-1} in the FT-IR spectrum of DEX_SUC. The peak at 893 cm^{-1} belongs to the C=O bond of the A ring of DEX which appears at 892 cm^{-1} in the FT-IR spectrum of DEX_SUC. The peak at 2950 cm^{-1} belongs to aliphatic C-H stretches of DEX which appears in 2951 cm^{-1} in the FT-IR spectrum of DEX_SUC. The broad peak at 3408 cm^{-1} belongs to OH stretches of alcoholic hydroxyl groups of DEX which appears at 3399 cm^{-1} in the FT-IR spectrum of DEX_SUC.

The characteristic peak at 1737 cm^{-1} in DEX-SUC FT-IR spectrum corresponding to the carboxylic carbonyl group of DEX_SUC disappears in the CHI_DEXs FT-IR spectra, which implies the formation of amide bond between DEX-SUC and CHI. After grafting DEX-SUC to CHI, the peaks at 1716 cm^{-1} (carbonyl group of esteric bond between DEX and SUC) and 1661 cm^{-1} (carbonyl group of DEX) in DEX_SUC FT-IR spectrum, shift a little and appear at 1718 and 1660 cm^{-1} in the FT-IR spectra of CHI_DEXs, respectively (Fig. 2d). As observed in Fig. 2d, with an increase in DS of the DEX_SUC on CHI, the intensities of these peaks obviously increases in the FT-IR spectra of CHI_DEXs. After grafting DEX-SUC to CHI, the intensity of the peak corresponding to the protonated amino groups of chitosan (NH_3^+) at 2039 cm^{-1} reduces due to reaction of these groups with the carboxyl group of DEX_SUC and shift to 2061 cm^{-1} in DEX-SUC FT-IR spectrum. Following this attachment, the peaks at 2887 and 2930 cm^{-1} belonging to the aliphatic CH3 and CH2 groups of CHI, respectively shift to 2889 and 2932 cm^{-1}, respectively and their intensity increases since grafting each DEX_SUC molecule to CHI, adds three CH3 and six CH2 groups to the structure. The broad peak at 3437 cm^{-1} in CHI FT-IR spectrum which appears in 3427 cm^{-1} in DEX_CHI FT-IR spectrum, belongs to the stretching vibration of NH_2 and OH groups. The peak at 1073 cm^{-1} in CHI FT-IR spectrum which appears in 1071 cm^{-1} in the DEX_CHI FT-IR spectrum, belongs to C-O stretch bond. The peak at 1635 cm^{-1} in CHI FT-IR spectrum which belongs to C=O bond of acetyl groups of CHI appears at 1635 cm^{-1} in the DEX_CHI FT-IR spectrum.

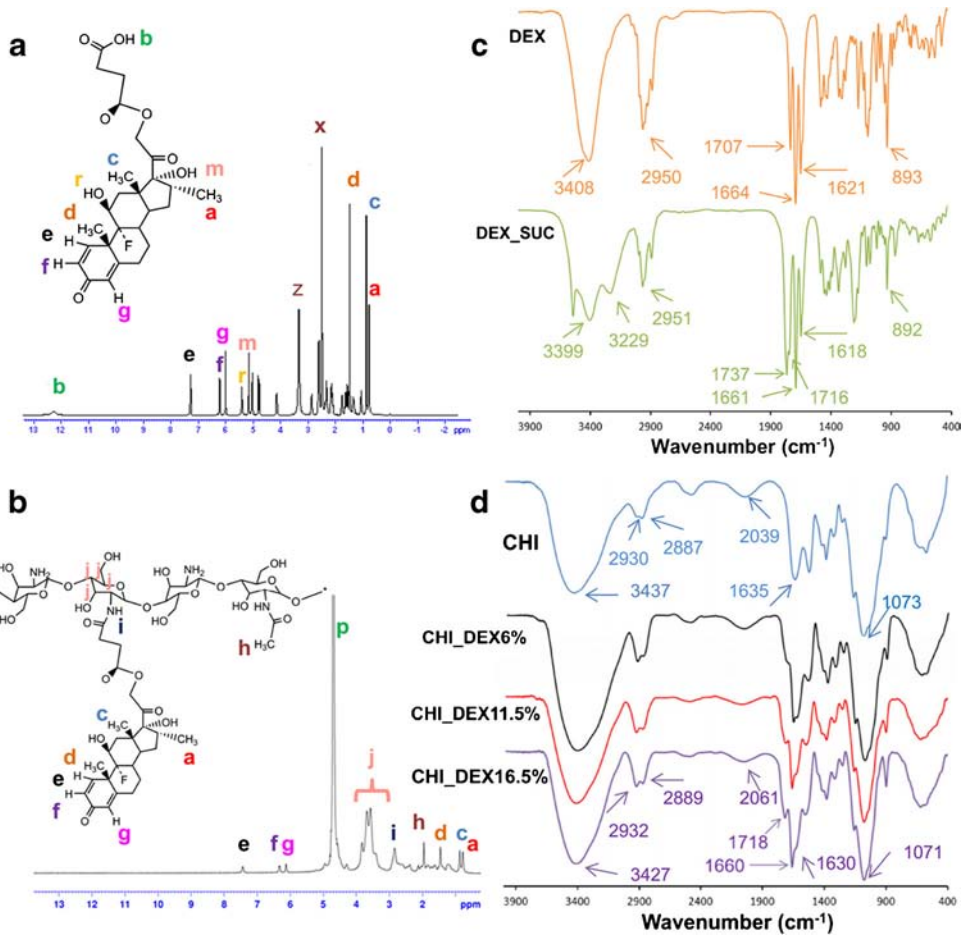

Fig. 2 (**a**) ^{1}HNMR spectrum of DEX-SUC in DMSO-d_6; (**b**) ^{1}HNMR spectrum of CHI_DEX11.5% in D_2O; (**c**) FT-IR spectra of DEX and DEX-SUC; and (**d**) FT-IR spectra of CHI, CHI_DEX6%, CHI_DEX11.5% and CHI_DEX16.5%.

Experimental Characterization of Micelles

The TEM images (Fig. 3) illustrate near spherical shape CBPMs with the size smaller than that of the one determined by DLS (Table II). This is mainly due to the fact that TEM determines micelles size at the dried state of the sample whereas the DLS determines the size in the hydrated state of the sample (30–32).

Since it takes up to 11 days for the CBPMs to accumulate in the tumor site following iv injection (33), a proper self-assembly tendency is necessary for the CHI amphiphilic derivatives to prevent dissociation of the CBPMs in the blood circulation before reaching their target site. Therefore, the CAC value, which is considered as a criterion for the self-assembly tendency of micelles (34,35), is measured for the CHI_DEXs through fluorescence spectroscopy using pyrene as a fluorescence probe. There exist five vibrational peaks in the pyrene fluorescence emission spectra (9). The intensity ratio of the first peak at 371 nm to the third peak at 390 nm (I_{371}/I_{390}) is sensitive to the polarity of the environment. As seen in Fig. 4, an increase in the polymer concentration which reduces the polarity of the environment through formation of hydrophobic microdomains, increases the intensity of the third peak (I_{390}) more than that of the first peak (I_{371}). Based on the changes of the I_{371}/I_{390} as a function of the different concentrations of CHI_DEXs, the CAC is measured. As

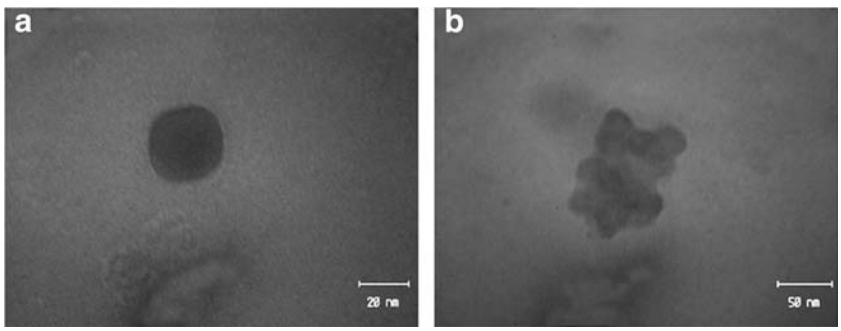

Fig. 3 TEM images of CHI_DEX11.5% polymeric micelles: (**a**) one micelle and (**b**) several micelles.

Table II CAC, Size and Zeta Potential of the Micelles Formed Through Self-Assembly of CHI_DEXs

CHI_DEXs	Diameter[a] (nm)	Zeta potential[b] (mV)	CAC[c] (mg/L)
CHI_DEX6%	335.5 ± 15.0	22.5 ± 1.1	1.5
CHI_DEX11.5%	370.9 ± 28.9	24.3 ± 2.2	2.7
CHI_DEX16.5%	273.6 ± 28.3	18.3 ± 2.0	0.9

[a] The size (mean value ± SD, $n = 3$)

[b] The zeta potential (mean value ± SD, $n = 3$)

[c] Critical aggregation concentration determined by fluorescence spectroscopy using the I_{371}/I_{390} data

observed in Table II, the lowest CAC value belongs to the CHI_DEX16.5%. CHI_DEX11.5% with two times more DS of the hydrophobic group than CHI_DEX6%, has a CAC value higher than that of CHI_DEX6%.

Since the therapeutic and diagnostic agents that are delivered by CBPMs are mainly used in cancer therapy, the tumor accumulation amount of CBPMs which is significantly affected by the micelles size (36) is considered as a determining factor in their capability of cancer therapy. Therefore, the change of micelles size in response to the change of DS of the hydrophobic group is evaluated experimentally. As observed in Table II, with an increase in DS of DEX from 6 to 11.5%, no significant change in the micelles size is observed while with further increase in DS of DEX from 11.5 to 16.5%, size of the micelles decreases. Although the results obtained in some other studies demonstrate that increasing hydrophobicity of a CHI amphiphilic derivative would cause it to form micelles with lower CAC value, smaller size (3,37–41) and lower zeta potential (39,40), evaluation of our experimental results reveal that increasing hydrophobicity of a CHI amphiphilic derivative would not necessarily cause it to form micelles with lower CAC value, smaller size and lower zeta potential.

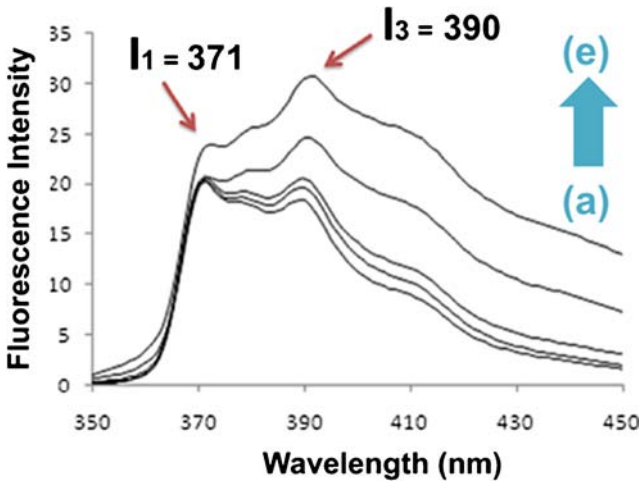

Fig. 4 Fluorescence spectra of pyrene (6×10^{-7}M) in CHI_DEX6% solutions with concentrations (mg/lit) of (**a**) 0.48, (**b**) 0.97, (**c**) 3.9, (**d**) 15.6 and (**e**) 31.2. (I_1 and I_3 are the first and third peaks in the pyrene fluorescence emission spectra).

As observed in Table II, with an increase in DS of DEX from 6 to 11.5%, no significant change is observed in zeta potential of micelles while, with an increase in DS of DEX from 11.5 to 16.5%, zeta potential decreases from 24.3±2.2 to 18.3±2.0 mV. When the DS of the hydrophobic group is increased, more amino groups of CHI enter the chemical reaction, thus the positive charge amount of polymeric chains reduces. This is the reason Du *et al.* mentioned to justify their results when they observed that the zeta potential of micelles reduced with an increase in DS of hydrophobic group (40). However, reduction of positive charge of CHI chains through hydrophobic modification, would not necessarily lead to the reduction of micelles zeta potential. The reason is that the zeta potential reflects micelles surface charge which in addition to the DS of the hydrophobic group, depends on some other factors such as size of the micelles, MW of CHI, and chemical structure of the hydrophobic group which is grafted to CHI.

Yuan *et al.* reported that the zeta potential of the CBPMs increased from 22.9±0.7 to 32.0±0.5 mV when the DS of stearoyl on CHI increased from 4.47±1.01 to 24.36±0.35. They believe that although an increase in DS of the hydrophobic group, would lead to a smaller amount of primary amino groups on the CHI, the smaller size of the micelles with higher DS would compensate for it. They mentioned that since the surface zeta potential of the micelles reflects the surface charge density, the smaller micelles would have higher surface charge density, thus a higher surface zeta potential (3).

Contrary to Yuan *et al.*, Wang *et al.* observed that the reduction of the size of CBPMs due to an increase in DS of the hydrophobic group, led to a decrease in the absolute value of micelles zeta potential. They concluded that this was perhaps due to more compact structure of the micelles with higher DS of the hydrophobic group which caused the amount of charged groups distributed on the surface of micelles to decrease (42).

There exist studies reporting that an increase in DS of the hydrophobic group would lead to a reduction in the size of the micelles without any significant change in the zeta potential (43,44). Chiu *et al.* reported that with an increase in DS of palmitoyl group on CHI from 5 to 20%, no significant change was observed in the zeta potential of micelles; while, the size reduced from 207.1±4.3 to 168.0±15.2 nm (44). Therefore, in addition to the amount of amino groups of CHI and the size of the micelles, there should be other factors affecting the zeta potential of micelles.

When the hydrophobic group stearoyl is grafted to two CHIs with different MWs of 5 and 18.7 kDa in an almost similar DS of around 25%, micelles with different size and zeta potential are obtained. The CHI chains with the MW of 5 kDa form micelles with the size of 66.2±7.9 nm and zeta potential of 32.0±0.5 mV (3) and the CHI chains with the

MW of 18.7 kDa, form micelles with the size of 27.4±2.4 nm and zeta potential of 51.7±3.0 mV (45).

Regarding CHIs with the same MW and DS of the hydrophobic group, the chemical structure of the hydrophobic group determines the size and zeta potential of the CBPMs. For example, when the linoleoyl group is grafted to 5 kDa CHI chains in a DS of 10.3%, the grafted CHI chains would form micelles with the size of 46.2±3.6 nm and zeta potential of 36.0±3.3 mV (7) and when the stearoyl group is grafted to 5 kDa CHI chains in a DS of 10.4%, the grafted CHI chains would form micelles with the size of 34.2±3.8 nm and zeta potential of 46.9±6.2 mV (46).

A high surface charge positive or negative would help the CBPMs to keep their stability through electrostatic repulsion force. However, a high surface charge would increase the risk of unspecific interactions of micelles with the plasma proteins. Accordingly, Zhou *et al.* designed CBPMs (glycidol-CHI-deoxycholic acid micelles) with the zeta potential almost near to zero in order to avoid the unspecific conjugation of micelles with proteins or enzymes by electrostatic interactions to increase circulation time of micelles *in vivo* (47). Therefore, it is essential to find the optimum zeta potential for the micelles in order to keep their stability in one hand and prevent their unspecified interactions on the other.

Although a high positive surface charge facilitates the adhesion of CBPMs to the negatively charged cell membranes, it is not the only factor affecting the interaction of micelles with the target cells. Hu *et al.* reported that a reduction in the zeta potential of stearic acid-grafted CHI micelles from 57.1±1.5 to 34.2±0.5 mV would not show a significant difference in micelles cellular uptake percentage. They concluded that the smaller size of micelles with 34.2±0.5 mV zeta potential compensated for their lower zeta potential (6).

Cellular uptake of negatively charged CBPMs (produced through grafting a negatively charged hydrophilic group like carboxy methyl (42,48) or sulfate (49) to CHI prior to hydrophobic modification), further proves that in addition to zeta potential, there are several other factors which affect micelles interactions with the target cells. Mekhail *et al.* reported a high amount of uptake of sulfated stearoyl CHI micelles by MCF 7 and HCT 116 cells (50). In addition to the zeta potential and size of the micelles, other factors such as DS of the hydrophobic group (44), concentration of the micelles and micelles incubation time with the cells (51) and the cell line type which the micelles are incubated with (6) are also essential in the amount of micelles cellular uptake.

Computational Results

Single-Chains Geometry

The atomistic MD simulations began by 50 ns simulations of the single-chain systems (CHI _1, CD6%_1, and CD11.5% _1, CD16.5% _1) to equilibrate their geometry in water. Clustering analysis was conducted on the last 10 ns of the single-chains trajectory to find their dominant conformation in the equilibrium phase. Average linkage algorithm implemented in ptraj module of Ambertools13 and a cluster count of 5 was used to get the optimum clustering results (24). The 500 conformations generated for each single-chain in the last 10 ns of its trajectory, were sorted in five clusters according to their similarity in RMSD. This sorting resulted in the percentage of the dominant cluster of 60.1% for CHI_1, 61.8% for CD6%_1, 69.3% for CD11.5%_1 and 60.4% for CD_16.5%_1. Each dominant cluster introduces a dominant conformation for each single chain (Fig. 5) which will be used for constructing the initial configuration of its hexamer system.

Since the self-assembly behavior of CHI_DEXs is significantly affected by the intra- and inter-chain interactions of the single-chains, the average SASA of the backbone and DEX residues of single-chains and their average buried SASA which are among the determining factors of these interactions are calculated for the equilibrated phase of the simulations (Table III).

The CHI_1 has an almost linear structure without any obvious folding (Fig. 5). This linear structure alters through grafting DEX to CHI. This structural alteration occurs due to the hydrophobic nature of DEX (see section "Local Behavior of Water Molecules Around CHI_DEXs"), which causes DEX residues to reduce their contact with water molecules through interacting with the backbone and/or other DEX residues. With respect to actual DS of DEX on CHI and actual length of CHI chain, the graft space (the space between two DEX residues) is approximately 18, 9 and 6 CHI monomers for CHI_DEX6%, CHI_DEX11.5% and CHI_DEX16.5%, respectively. In CD6%_1, due to large graft space of DEX residues, the possibility of intra-chain interactions between DEX residues is low, thus, the DEX residues mostly interact with the

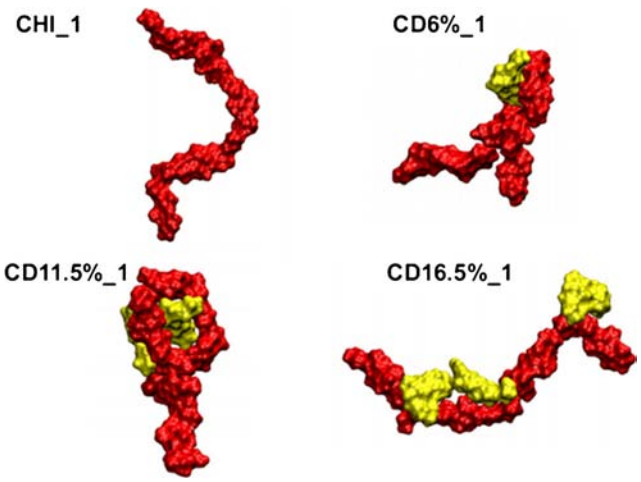

Fig. 5 SASA representation of the dominant conformation of the single-chains. The *red* and *yellow* colors refer to the backbone (CHI) and DEX residues, respectively.

backbone in a manner where 52.6±2.4% of the surface of DEX residues is buried under the backbone. Interactions between backbone and DEX residue partially fold the backbone in a manner where the backbone in CD6%_1 loses about 14% of its SASA compared to that of the CHI_1 (Table III). This partial folding causes 47.4±2.0% of DEX surface to remain accessible at the surface of the chain.

With an increase in DS of DEX from 6 to 11.5%, the graft space is reduced, causing an increase in the chance of intra-chain DEX-DEX interactions. These interactions together with DEX-backbone interactions, strongly fold the backbone in a manner where the backbone loses about 22% of its SASA compared to that of the CHI_1 which causes the CD11.5%_1 to have the most compacted conformation compared to that of the other three single-chain systems. This compacted conformation causes only 37.5±1.9% of DEX surface to remain accessible at the surface of the chain.

In CD16.5%_1 despite of the 16.5% DS of DEX, an extended conformation is observed. With respect to the CHI semi rigid structure, with an increase in DS of DEX residues from 11.5 to 16.5%, the short backbone length in the graft space would cause less conformational freedom for the backbone in CD16.5%_1 compared to the conformational freedom of the backbone in CD11.5%_1. Therefore, it is difficult for the neighboring DEX residues to fold the backbone in order to interact with each other and the backbone. This causes that in average 6.8±0.3% of the surface of each DEX residue is buried under other DEX residues and 37.5±1.8% of its surface is buried under the backbone. Therefore, in CD16.5%_1, 55.6±2.1% of the surface of each DEX residue remains accessible at the surface of the chain which would increase the self-assembly tendency of chains through formation of effective inter-chain interactions.

Self-Assembly Tendency of CHI_DEXs

To evaluate the self-assembly tendency of CHI_DEXs, 50 ns MD simulations are performed on the hexamer systems which their structure before and after 50 ns MD simulations are presented in Fig. 6. Here, only CD16.5%_6 remains hexamer during 50 ns MD simulation something that did not occur for the other systems due to ineffective inter-chain interactions. Formation of effective inter-chain interactions depends on many factors among which the inter-chain hydrophobic interactions are considered as the main driving force for the self-assembly of CHI_DEXs (see section "Self-assembly energy analysis"). The inter-chain hydrophobic interactions exert an optimum effect when the hydrophobicity-hydrophilicity balance (HHB) of the chain reaches an optimum amount. Here, the ratio of the hydrophobic to the hydrophilic SASA of the single-chains is used as an index for the HHB. The ratio of the hydrophobic to the hydrophilic SASA of CHI_1 is 73.5±3.1% (Table III) indicating that the CHI has an amphiphilic nature. However, the hydrophobicity of CHI chains does not provide enough hydrophobic inter-chain interactions for the self-assembly in concentrations lower than 1 mg/ml (52). Through hydrophobic modification of CHI with DEX molecules, we increased the HHB of the CHI chain towards more hydrophobicity.

In order to demonstrate the necessity of hydrophobic modification of CHI for the formation of effective hydrophobic interactions, we evaluate the residence time of pyrene as a hydrophobic probe (with the ratio of hydrophobic to the total SASA of 100%) on the surface of the CHI_DEXs' single-chains (Fig. 7a). Due to the lack of significant hydrophobic groups in the CHI structure, the CHI_1_P complex remains stable for less than 1 ns, while, the CD6%_1_P, CD11.5%_1_P and CD16.5%_1_P complexes keep their stability for longer simulation times. Observation of pyrene in contact with the DEX residue (Fig. 7b) indicates the importance of the hydrophobic

Table III Average SASA and Buried SASA of DEX and Backbone in Single-Chain Systems and CD16.5%_6 Over the Last 10 ns of the MD Simulations

Systems	Total SASA (Å^2)	Backbone SASA (Å^2)	The ratio of the hydrophobic to the hydrophilic SASA (%)[a]	Relative accessibility of DEX residues[b] (%)	DEX-DEX buried SASA [c](%)	DEX-backbone buried SASA[d] (%)
CHI_1	3163.4±151.2	3163.9±151.2	73.5±3.1	–	–	–
CD6%_1	3095.3±123.7	2734.2±126.5	83.3±3.9	47.4±2.0	–	52.6±2.4
CD11.5%_1	3052.8±161.6	2478.5±129.7	103.0±5.3	37.5±1.9	17.4±0.9	45.6±2.3
CD16.5%_1	4046.8±183.3	2772.6±122.6	108.1±5.1	55.6±2.1	6.8±0.3	37.5±1.8
CD16.5%_6	16945.6±798.8	1993.1[e]±90.6	nc[f]	36.3±1.7	nc[f]	nc[f]

[a] The ratio of the average SASA of the non-polar atoms to the polar atoms

[b] Average SASA of DEX residues / SASA of a free DEX molecule

[c] Average buried SASA of each DEX between DEX residues

[d] Average buried SASA of each DEX residue under the backbone

[e] Average SASA for the backbone of the six chains

[f] Not calculated

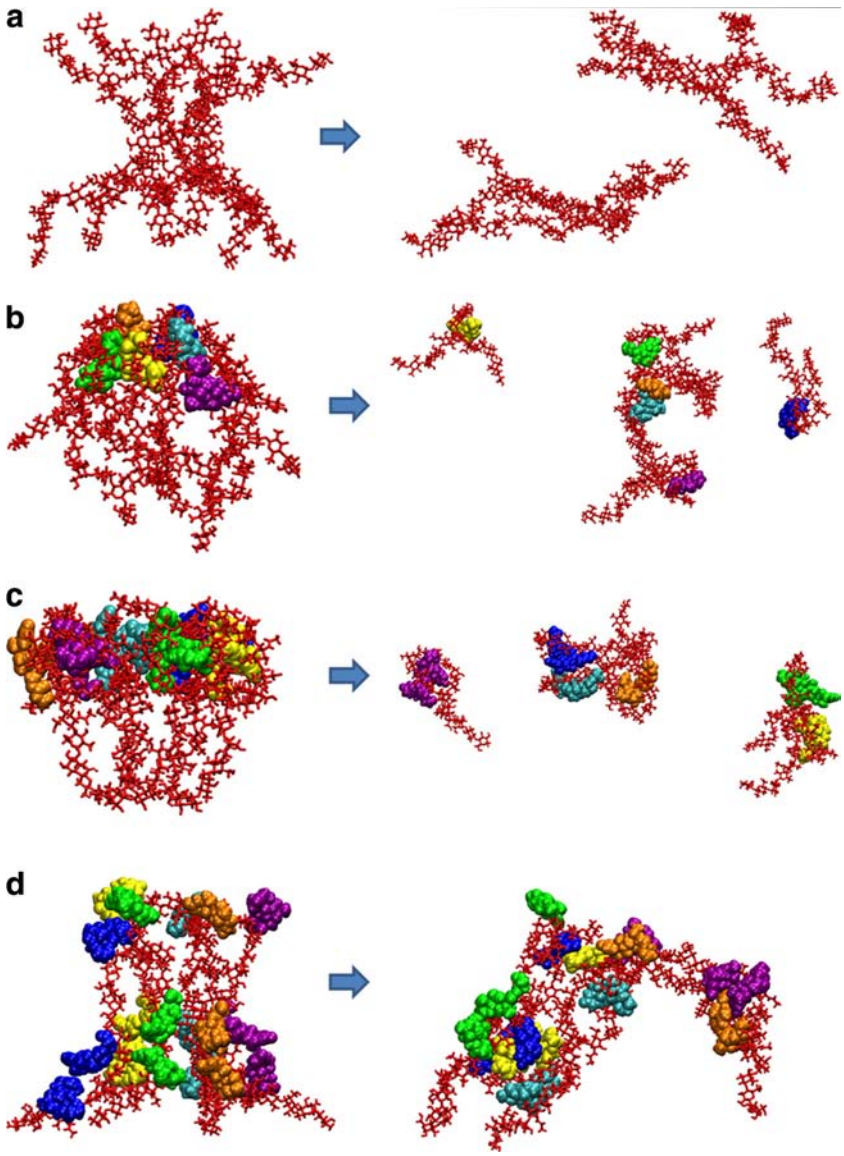

Fig. 6 Self-assembly tendency of the hexamer systems: (**a**) CHI_6, (**b**) CD6%_6, (**c**) CD11.5%_6 and (**d**) CD16.5%_6. Here, the left and right sides represent before and after 50 ns MD simulations, respectively. Space filling parts represent the DEX residues where they are presented by their unique color in each chain in order to facilitate the observation of inter-chain DEX-DEX interactions and hydrophobic microdomains distribution.

modification of CHI in enabling CHI amphiphilic derivatives to form effective hydrophobic interactions.

Although the HHB of CHI is increased towards more hydrophobicity through grafting DEX to CHI, the optimum HHB is gained in a certain DS of the hydrophobic group. In the CD6%_1 the ratio of the hydrophobic to the hydrophilic SASA increases to 83.3±3.9% and the surface accessibility of DEX residues is 47.4±2.0% but dissociation of its hexamer during 50 ns MD simulation indicates that CD6%_1 has no optimum HHB. In CD11.5%_1, while the ratio of the hydrophobic to the hydrophilic SASA increases to 103.0±5.3%, the effective intra-chain interactions cause the polymeric chain to form a compacted conformation (see the section "Single-chains Geometry") which makes it difficult for its hexamer to remain stable (Fig. 6c).

Among the three DSs used, DS of 16.5% provides a more optimum HHB and an extended conformation for the chains (see the section "Single-chains Geometry") which increase the possibility of effective inter-chain interactions. These interactions would cause the chains to demonstrate a strong self-assembly tendency where the average SASA of the backbone in CD16.5%_6 is smaller by 28% than that of the CD16.5%_1, and the relative accessibility of DEX residues reduces from 55.6±2.1% in CD16.5%_1 to 36.3±1.7% in CD16.5%_6.

Despite the reduction of relative accessibility of DEX molecules during the process of self-assembly of CD16.5%_6, 36.3±1.7% of DEX residues surface is still accessible at the surface of the chains. Therefore, in addition to the role of DEX in the self-assembly of chains, the DEX residues can also interact with biological membranes both passively through hydrophobic interactions and actively through glucocorticoid receptors which would lead to the facilitation of the membrane trafficking of the micelles in order to deliver their

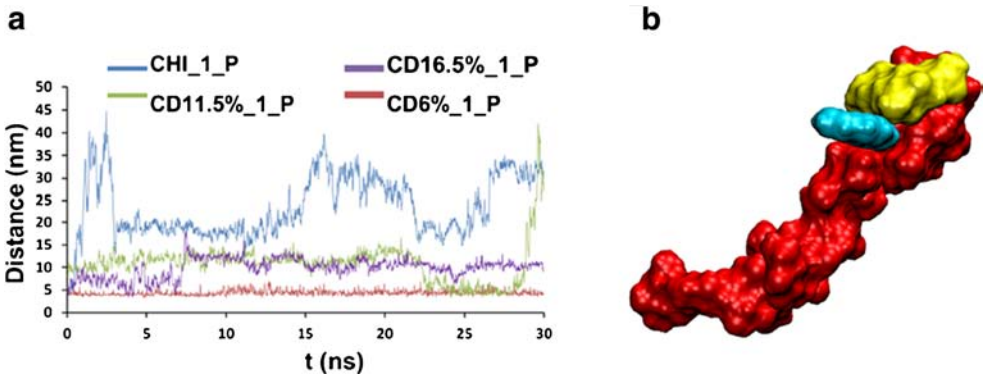

Fig. 7 (**a**) Residence time of pyrene on the surface of CHI and CHI_DEXs single-chains; (**b**) CD6%_1_P after 30 ns MD simulation: *blue*, *yellow* and *red* colors refer to pyrene, DEX and CHI, respectively.

content to the site of action. Unlike CBPMs, in case of micelles formed by self-assembly of block copolymers where the hydrophobic segments associate in the core and are segregated from outer medium by the hydrophilic shell (53), the hydrophobic segments do not directly take part in biological interactions of micelles with the membranes.

Regarding CBPMs, hydrophobic groups are smaller than the backbone and are grafted to a number of points along the backbone. During the self-assembly process, these hydrophobic groups do not form a hydrophobic core since besides their smaller size compared to the backbone, the hydrophobic residues cannot behave independent of the backbone. Therefore, instead of formation of a classic core-shell structure, CBPMs form hydrophobic microdomains spread among the lattice of CHI chains (Fig. 6d). These hydrophobic microdomains have no uniform structure composed only of hydrophobic groups and sometimes a part of the backbone or a cavity in structure accompany the hydrophobic groups in the formation of hydrophobic microdomains.

Since among the hexamer systems, only CD16.5%_6 remained stable during 50 ns MD simulation, the radial distribution function (RDF), MM-GBSA and Hbonds analyses are performed on this system.

The Balance of Intra- and Inter-Chain Interactions

From the two previous sections, it is deduced that there exists a balance between intra- and inter-chain interactions which significantly affects the self-assembly behavior of the CHI_DEXs (Fig. 8).

To evaluate this balance in a greater scale, a 50 ns MD simulation is conducted on a system composed of 30 chains. Due to the effective intra-chain interactions in the CD11.5%_1 which would make it difficult for its hexamer to remain stable, these chains are selected for this simulation. In Fig. 9 and the video animation (see the supplementary materials) of the trajectory of this MD simulation, no aggregate larger than tetramer is observed and nearly one-third of the chains are in the form of unimers. In parallel to this

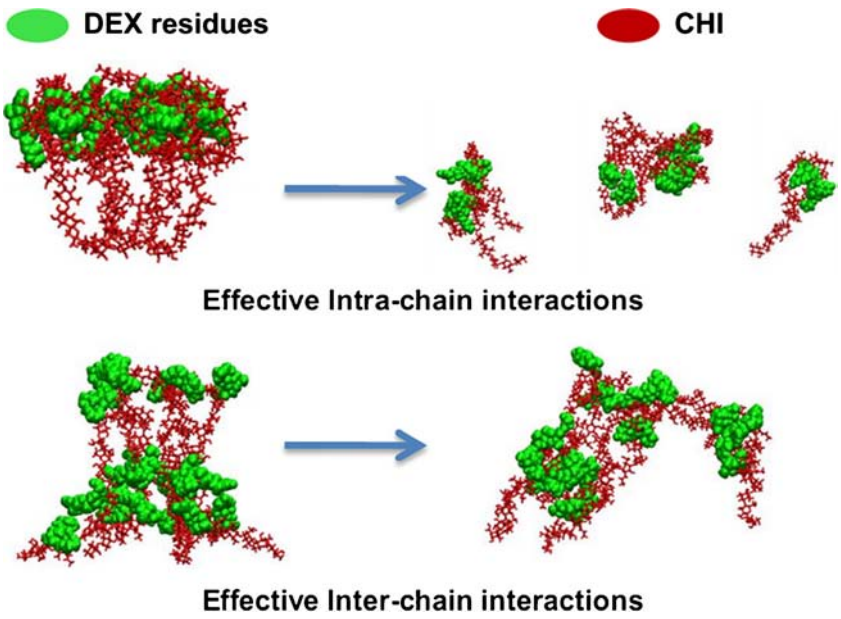

Fig. 8 The balance between intra- and inter-chain interactions affects the self-assembly behavior of CHI_DEXs.

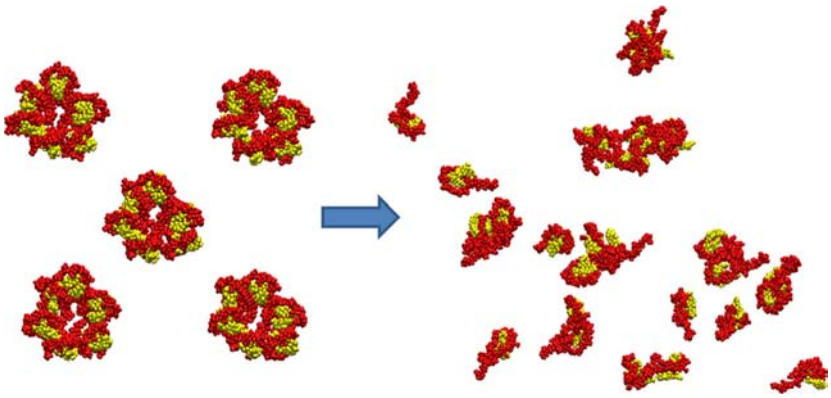

Fig. 9 Self-assembly tendency in the CD11.5%_30 system during 50 ns MD simulation. Here, the left and right sides represent before and after 50 ns MD simulation, respectively. The *red* and *yellow* colors refer to the backbone and DEX residues, respectively.

observation, due to effective inter-chain interactions, even six chains of CD16.5% remained as a hexamer during 50 ns MD simulation (Fig. 6d). Therefore, in case the balance between intra- and inter-chain interactions is shifted to either side, the tendency of chains for self-assembly and consequently the CAC, size and zeta potential of the micelles are greatly affected.

Self-Assembly Energy Analysis

To determine the role of contributing energies in the enthalpy of the self-assembly process, the MM-GBSA analysis is performed on two (out of six) chains of the CD16.5%_6. Although the values of the contributing energies are different for the two chains, the role and the ratio of the contributing energies are almost the same for both of them (Table IV). An investigation of the self-assembly energy components reveals that the contribution of the electrostatic energy (ΔE_{ele}) in the self-assembly of chains is unfavorable. It should be noted that although inter-chain Hbonds have a constructive role in the process of self-assembly, they are compensated with the strong repulsion forces among protonated amino groups of CHI.

Despite the high negative value of the electrostatic desolvation penalty ($\Delta G_{sol\text{-}polar}$) which mostly offsets the unfavorable (positive) inter-chain electrostatic forces, an unfavorable net polar contribution (ΔG_{polar}) still remains against self-assembly of the chains. Unfavorable inter-chain electrostatic forces arise mostly from strong inter-chain electrostatic repulsion among protonated amino groups of the backbone. These repulsive interactions cause the CAC of CBPMs to increase through a decrease in the medium pH (54), since at a lower pH more amino groups are protonated which makes the chains aggregation more difficult. Therefore, the DS of the Hydrophobic group can affect the ΔE_{ele} by altering the ratio of the protonated amines. In a higher DS, more amino groups enter the chemical reaction, thus lower amount of unreacted free amino groups remain to be protonated. The remainder of the unfavorable net polar contribution is compensated by favorable nonpolar or hydrophobic component contributors ($\Delta G_{non\text{-}polar}$) which make them as the main driving force for self-assembly of CHI_DEXs. Although conformational entropy changes ($-T\Delta S$) can partially offset the self-assembly enthalpy changes ($\Delta H_{self\text{-}assembly}$), the self-assembly free energy ($\Delta G_{self\text{-}assembly}$) still remains negative.

Table IV Calculated Self-Assembly Enthalpy and Its Components (kcal/mol) for Two (Out of Six) Chains of CD16.5%_6

Energy contributions	Chain A	Chian B
ΔE_{vdw}	−207.78	−194.34
ΔE_{ele}	1490.56	1240.72
ΔG_{sol_polar}	−1347.53	−1126.14
$\Delta G_{sol\_nonpolar}$	−22.65	−21.90
ΔG_{non_polar} [a]	−230.43	−216.24
ΔG_{polar} [b]	143.03	114.58
$\Delta H_{self\text{-}assembly}$	−87.41	−101.65
$-T\Delta S$	46.63	61.83
$\Delta G_{self\text{-}assembly}$ [c]	−40.77	−39.82

[a] $\Delta G_{non\_polar} = \Delta E_{vdw} + \Delta G_{sol\_nonpolar}$

[b] $\Delta G_{polar} = \Delta E_{ele} + \Delta G_{sol\_polar}$

[c] $\Delta G_{self\text{-}assembly} = \Delta H_{self\text{-}assembly} - T\Delta S$

Local Behavior of Water Molecules Around the Polymeric Chains

RDF analysis is performed to investigate the local behavior of water molecules around the CHI_DEXs. Figure 10a shows the distribution pattern of water oxygens (OW) around the central carbon of DEX residue and oxygen of hydroxyl groups of backbone in CD16.5%_1 and CD16.5%_6. RDF analysis is conducted on the last 10 ns of the MD simulations. The first peak for the backbone appears around 2.7 Å and the second peak around 5.3 Å corresponding to the first and second hydration shells, respectively. For the DEX residue, an inconspicuous peak appears around 4.7 Å indicating that the DEX residue is much more hydrophobic than the backbone.

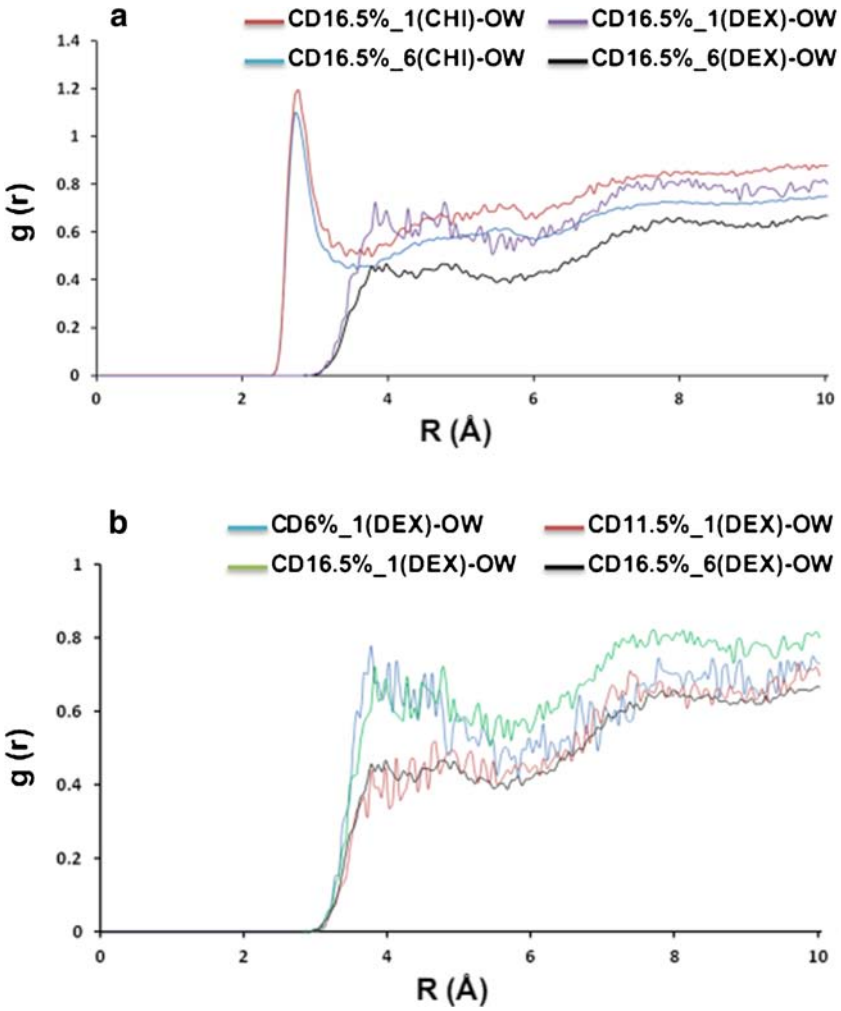

Fig. 10 RDF for (**a**) CHI oxygen-OW and central carbon of DEX-OW in CD16.5%_1 and CD16.5%_6 (**b**) central carbon of DEX-OW in single-chain systems and CD16.5%_6.

Since some of the water molecules are repelled from the surface of the chains during the self-assembly process, the RDF peaks heights of both the backbones and DEX residues of CD16.5%_6 are lower than that of the CD16.5%_1. This is more evident for the DEX residues in comparison with the backbones, since according to the SASA results, the ratio of the hydrophobic to the total surface area of DEX molecule is 73.6±2.2% while this value is 42.2±1.7% for the CHI.

As seen in Fig. 10b, the peak height of DEX residues in CD11.5%_1 is much lower than that of the CD6%_1 and CD16.5%_1 and in fact is approximately equal to that of the CD16.5%_6. The SASA results confirm this observation indicating that the solvent accessibility of DEX residues in CD11.5%_1 is almost the same as that of the DEX residues in CD16.5%_6. Therefore, the DEX residues of CD11.5%_6 cannot form effective inter-chain interactions. Despite the higher RDF peak and more surface accessibility of DEX residue in CD6%_1 in comparison with the CD11.5%_1, the CD6%_6 chains cannot supply effective inter-chain interactions (see the sections "Single-Chains Geometry" and "Self-Assembly Tendency of CHI_DEXs").

Hbonds Role in the Self-Assembly Process of CHI_DEXs

To elucidate the Hbonds role in the self-assembly process of CHI_DEXs chains, Hbonds analysis was conducted on the CD16.5%_1 and CD16.5%_6. This analysis revealed that the Hbonds play both the destructive and constructive roles in the chains self-assembly process depending on whether the Hbonds are between polymeric chains and water molecules or between polymeric chains, respectively. As seen in Fig. 11a, the average number of Hbonds of CD16.5%_1 with water in the last 2 ns of the MD simulation is 87.77. This is while the average number of chain-water Hbonds for each chain of CD16.5%_6 decreases during the process of self-assembly and reduces to 77.98 in the last 2 ns of the MD simulation (Fig. 11b) indicating that chain-water Hbonds are destructive to the self-assembly process. The constructive role of Hbonds to the self-assembly process can be concluded from observing Fig. 11c where the average number of inter-chain Hbonds in CD16.5%_6 increases from 0.9 in the first 2 ns of the MD simulation to 3.73 in the last 2 ns of the MD simulation.

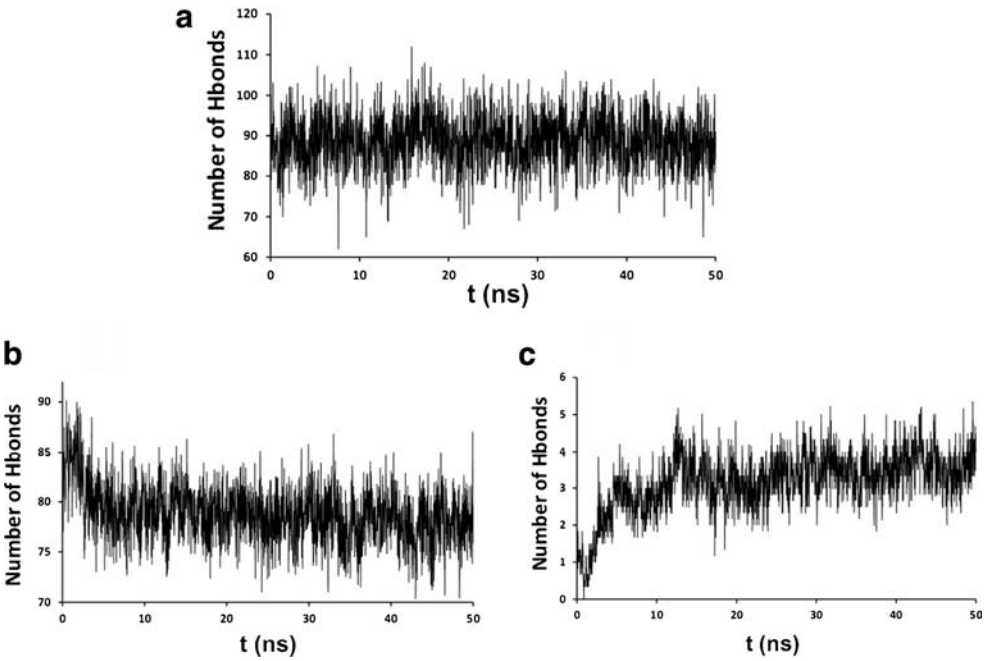

Fig. 11 The Hbonds role in the self-assembly process of CHI_DEXs during the MD simulation. (**a**) number of Hbonds of CD16.5%_1 with water; (**b**) average number of chain-water Hbonds for each chain of CD16.5%_6 and (**c**) average number of inter-chain Hbonds for every CD16.5%_6 chain.

CONCLUSION

In this study, the graft of DEX molecules to the CHI, provided CHI_DEXs chains with the capability of self-assembly. The CAC, size and zeta potential of the micelles formed through self-assembly of these new CHI derivatives were measured and compared so that the self-assembly behavior of these micelles is evaluated. Our evaluation of the experimental results reveals that increasing hydrophobicity of a CHI amphiphilic derivative would not necessarily cause it to form micelles with lower CAC value, smaller size and lower zeta potential. Since the use of MD simulations together with the experiment, facilitates elucidation of the molecular mechanisms behind this self-assembly behavior of CHI_DEXs, thorough MD simulations were performed on CHI_DEXs.

Our MD simulations reveal that an increase in DS of the hydrophobic group triggers a cascade of molecular events that shifts the balance between intra- and inter-chain interactions leading to changes in the CAC, size and zeta potential of the CBPMs (Fig. 12). An increase in DS of the hydrophobic group alters the single-chains geometry where this geometrical alteration alongside the direct effect of the DS of the hydrophobic group, change the HHB of the single-chains. The resultant of the effects of the HHB of the single-chains and the single-chains geometry on the balance between the intra- and inter-chain interactions, shifts the balance toward intra- or inter-chain interactions. This means that an increase in DS, may not necessarily shift the balance toward inter-chain interactions to form micelles with a smaller size and a lower CAC value. For instance, regarding CHI_DEXs, as DS increases from 6 to 11.5%, single-chains conformation becomes compacted and HHB is increased by 19.7%. The resultant of the effects of these changes on the balance between intra- and inter-chain interactions shifts the balance towards intra-chain interactions leading to an increase in size and CAC of micelles. With an increase in DS from 11.5 to 16.5%, the single chain conformation becomes expanded and HHB is increased by 5%. Now, the resultant of the effects of these changes shifts the balance between intra- and inter-chain interactions towards inter-chain interactions leading to a decrease in size and CAC of micelles.

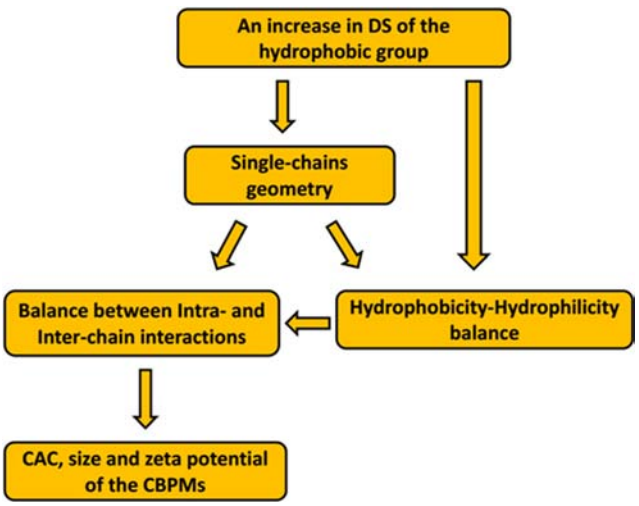

Fig. 12 Cascade of molecular events that is triggered by an increase in DS of the hydrophobic group that shifts the balance between intra- and inter-chain interactions leading to changes in the CAC, size and zeta potential of the CBPMs.

In addition to DS of the hydrophobic group, the self-assembly behavior of CHI amphiphilic derivatives depends to many other factors such as chemical structure of the hydrophobic group, DS of the hydrophilic group, chemical structure of the hydrophilic group and the ratio of the hydrophobic to the hydrophilic group. For example, dependency of self-assembly behaviour of CHI amphiphilic derivatives to the chemical structure of the hydrophobic group is revealed when linoleoyl grafted CHI chains and stearoyl grafted CHI chains demonstrate different self-assembly behavior even in an almost the same DS of the hydrophobic group of 10.3% for linoleoyl and 10.4% for stearoyl groups. Linoleoyl grafted CHI chains form micelles with the size of 46.2±3.6 nm and zeta potential of 36.0±3.3 mV (7) and stearoyl grafted CHI chains form micelles with the size of 34.2±3.8 nm and zeta potential of 46.9±6.2 mV (46). This is while almost the similar CAC values of 86.69 μg/mL and 90.07 μg/mL was reported for the micelles formed through self-assembly of linoleoyl grafted CHI chains (7) and stearoyl grafted CHI chains (46), respectively. Therefore, thorough evaluation of the self-assembly behavior of CHI amphiphilic derivatives and elucidation of all molecular mechanisms behind it, needs multiple studies to be conducted on all the factors that affect self-assembly behavior of CHI amphiphilic derivatives.

ACKNOWLEDGMENTS AND DISCLOSURES

This work was financially supported in part by Isfahan University of Medical Sciences (research project No.388492) and in part by Shakhes Pajouh Research Institute, Isfahan, Iran. The authors would like to thank Shohreh Hooshmandrad, Alireza Shahnooshi, Marzieh Akbari and Elahe Moazzen for their technical assistance in the experimental stage. We appreciate Mr. Haidoak Vartevan's assistance in proofreading the manuscript.

REFERENCES

1. Yan J, Du Y-Z, Chen F-Y, You J, Yuan H, Hu F-Q. Effect of proteins with different isoelectric points on the gene transfection efficiency mediated by stearic acid grafted chitosan oligosaccharide micelles. Mol Pharm. 2013;10(7):2568–77.
2. Na JH, Koo H, Lee S, Min KH, Park K, Yoo H, *et al.* Real-time and non-invasive optical imaging of tumor-targeting glycol chitosan nanoparticles in various tumor models. Biomaterials. 2011;32(22):5252–61.
3. Yuan H, Lu L-J, Du Y-Z, Hu F-Q. Stearic acid-g-chitosan polymeric micelle for oral drug delivery: in vitro transport and in vivo absorption. Mol Pharm. 2010;8(1):225–38.
4. Mahmoudzadeh M, Fassihi A, Emami J, Davies NM, Dorkoosh F. Physicochemical, pharmaceutical and biological approaches toward designing optimized and efficient hydrophobically modified chitosan-based polymeric micelles as a nanocarrier system for targeted delivery of anticancer drugs. J Drug Target. 2013;21(8):693–709.
5. Kean T, Thanou M. Biodegradation, biodistribution and toxicity of chitosan. Adv Drug Deliv Rev. 2010;62(1):3–11.
6. Hu FQ, Wu X, Du YZ, You J, Yuan H. Cellular uptake and cytotoxicity of shell crosslinked stearic acid-grafted chitosan oligosaccharide micelles encapsulating doxorubicin. Eur J Pharm Biopharm. 2008;69(1):117–25.
7. Du Y-Z, Wang L, Yuan H, Hu F-Q. Linoleic acid-grafted chitosan oligosaccharide micelles for intracellular drug delivery and reverse drug resistance of tumor cells. Int J Biol Macromol. 2011;48(1):215–22.
8. McLeod AD, Friend DR, Tozer TN. Synthesis and chemical stability of glucocorticoid-dextran esters: potential prodrugs for colon-specific delivery. Int J Pharm. 1993;92(1–3):105–14.
9. Yinsong W, Lingrong L, Jian W, Zhang Q. Preparation and characterization of self-aggregated nanoparticles of cholesterol-modified O-carboxymethyl chitosan conjugates. Carbohydr Polym. 2007;69(3):597–606.
10. Pillai C, Paul W, Sharma CP. Chitin and chitosan polymers: chemistry, solubility and fiber formation. Prog Polym Sci. 2009;34(7):641–78.
11. Case D, Darden T, Cheatham III T, Simmerling C, Wang J, Duke R, *et al.* AMBER 12. San Francisco: University of California; 2012.
12. Wang J, Wang W, Kollman PA, Case DA. Automatic atom type and bond type perception in molecular mechanical calculations. J Mol Graph Model. 2006;25(2):247–60.
13. Wang J, Wolf RM, Caldwell JW, Kollman PA, Case DA. Development and testing of a general amber force field. J Comput Chem. 2004;25(9):1157–74.
14. Jakalian A, Jack DB, Bayly CI. Fast, efficient generation of high quality atomic charges. AM1-BCC model: II. Parameterization and validation. J Comput Chem. 2002;23(16):1623–41.
15. Jakalian A, Bush BL, Jack DB, Bayly CI. Fast, efficient generation of high quality atomic Charges. AM1-BCC model: I. Method. J Comput Chem. 2000;21(2):132–46.
16. Feller SE, Zhang Y, Pastor RW, Brooks BR. Constant pressure molecular dynamics simulation: the Langevin piston method. J Chem Phys. 1995;103(11):4613–21.
17. Darden T, York D, Pedersen L. Particle mesh Ewald: AN N• log (N) method for Ewald sums in large systems. J Chem Phys. 1993;98(12):10089–92.
18. Ryckaert J-P, Ciccotti G, Berendsen HJ. Numerical integration of the cartesian equations of motion of a system with constraints: molecular dynamics of n-alkanes. J Comput Phys. 1977;23(3):327–41.
19. Salomon-Ferrer R, Götz AW, Poole D, Le Grand S, Walker RC. Routine microsecond molecular dynamics simulations with amber on GPUs. 2. Explicit solvent particle mesh Ewald. J Chem Theory Comput. 2013;9(9):3878–88.
20. Humphrey W, Dalke A, Schulten K. VMD: visual molecular dynamics. J Mol Graph. 1996;14(1):33–8.
21. Hubbard SJ, Thornton JM. Naccess. Computer program, Department of Biochemistry and Molecular Biology, University College London. 1993;2(1).
22. Velinova M, Sengupta D, Tadjer AV, Marrink S-J. Sphere-to-rod transitions of nonionic surfactant micelles in aqueous solution modeled by molecular dynamics simulations. Langmuir. 2011;27(23):14071–7.
23. Lee M-T, Vishnyakov A, Neimark AV. Calculations of critical micelle concentration by dissipative particle dynamics simulations: the role of chain rigidity. J Phys Chem B. 2013;117(35):10304–10.
24. Shao J, Tanner SW, Thompson N, Cheatham TE. Clustering molecular dynamics trajectories: 1. Characterizing the performance of different clustering algorithms. J Chem Theory Comput. 2007;3(6):2312–34.

25. Morris GM, Huey R, Lindstrom W, Sanner MF, Belew RK, Goodsell DS, *et al.* AutoDock4 and AutoDockTools4: automated docking with selective receptor flexibility. J Comput Chem. 2009;30(16):2785–91.
26. Kollman PA, Massova I, Reyes C, Kuhn B, Huo S, Chong L, *et al.* Calculating structures and free energies of complex molecules: combining molecular mechanics and continuum models. Acc Chem Res. 2000;33(12):889–97.
27. Srinivasan J, Cheatham TE, Cieplak P, Kollman PA, Case DA. Continuum solvent studies of the stability of DNA, RNA, and phosphoramidate-DNA helices. J Am Chem Soc. 1998;120(37): 9401–9.
28. Sitkoff D, Sharp KA, Honig B. Accurate calculation of hydration free energies using macroscopic solvent models. J Phys Chem. 1994;98(7):1978–88.
29. Chong LT, Duan Y, Wang L, Massova I, Kollman PA. Molecular dynamics and free-energy calculations applied to affinity maturation in antibody 48G7. Proc Natl Acad Sci. 1999;96(25):14330–5.
30. Wang YS, Liu LR, Jiang Q, Zhang QQ. Self-aggregated nanoparticles of cholesterol-modified chitosan conjugate as a novel carrier of epirubicin. Eur Polym J. 2007;43(1):43–51.
31. Wang F, Zhang D, Duan C, Jia L, Feng F, Liu Y, *et al.* Preparation and characterizations of a novel deoxycholic acid–O-carboxymethylated chitosan–folic acid conjugates and self-aggregates. Carbohydr Polym. 2011;84(3):1192–200.
32. Liu C-G, Desai KGH, Chen X-G, Park H-J. Linolenic acid-modified chitosan for formation of self-assembled nanoparticles. J Agric Food Chem. 2005;53(2):437–41.
33. Cho YW, Kim Y, Kim I, Park R, Oh SJ, Moon DH, *et al.* Tumoral accumulation of long-circulating, self-assembled nanoparticles and its visualization by gamma scintigraphy. Macromol Res. 2008;16(1):15–20.
34. Moretton MA, Glisoni RJ, Chiappetta DA, Sosnik A. Molecular implications in the nanoencapsulation of the anti-tuberculosis drug rifampicin within flower-like polymeric micelles. Colloids Surf B: Biointerfaces. 2010;79(2):467–79.
35. Li T, Lin J, Chen T, Zhang S. Polymeric micelles formed by polypeptide graft copolymer and its mixtures with polypeptide block copolymer. Polymer. 2006;47(13):4485–9.
36. Cho YW, Park SA, Han TH, Son DH, Park JS, Oh SJ, *et al.* In vivo tumor targeting and radionuclide imaging with self-assembled nanoparticles: mechanisms, key factors, and their implications. Biomaterials. 2007;28(6):1236–47.
37. Jiang G-B, Quan D, Liao K, Wang H. Novel polymer micelles prepared from chitosan grafted hydrophobic palmitoyl groups for drug delivery. Mol Pharm. 2006;3(2):152–60.
38. Jiang GB, Quan D, Liao K, Wang H. Preparation of polymeric micelles based on chitosan bearing a small amount of highly hydrophobic groups. Carbohydr Polym. 2006;66(4):514–20.
39. Fattahi A, Golozar M-A, Varshosaz J, Sadeghi HM, Fathi M. Preparation and characterization of micelles of oligomeric chitosan linked to all-trans retinoic acid. Carbohydr Polym. 2012;87(2): 1176–84.
40. Du Y-Z, Wang L, Yuan H, Wei X-H, Hu F-Q. Preparation and characteristics of linoleic acid-grafted chitosan oligosaccharide micelles as a carrier for doxorubicin. Colloids Surf B: Biointerfaces. 2009;69(2):257–63.
41. Elsabee MZ, Morsi RE, Al-Sabagh A. Surface active properties of chitosan and its derivatives. Colloids Surf B: Biointerfaces. 2009;74(1):1–16.
42. Wang Y, Yang X, Yang J, Wang Y, Chen R, Wu J, *et al.* Self-assembled nanoparticles of methotrexate conjugated O-carboxymethyl chitosan: preparation, characterization and drug release behavior in vitro. Carbohydr Polym. 2011;86(4):1665–70.
43. Yuan X, Li H, Yuan Y. Preparation of cholesterol-modified chitosan self-aggregated nanoparticles for delivery of drugs to ocular surface. Carbohydr Polym. 2006;65(3):337–45.
44. Chiu YL, Ho YC, Chen YM, Peng SF, Ke CJ, Chen KJ, *et al.* The characteristics, cellular uptake and intracellular trafficking of nanoparticles made of hydrophobically-modified chitosan. J Control Release. 2010;146(1):152–9.
45. Ye YQ, Yang FL, Hu FQ, Du YZ, Yuan H, Yu HY. Core-modified chitosan-based polymeric micelles for controlled release of doxorubicin. Int J Pharm. 2008;352(1–2):294–301.
46. Huang S-T, Du Y-Z, Yuan H, Zhang X-G, Miao J, Cui F-D, *et al.* Synthesis and anti-hepatitis B virus activity of acyclovir conjugated stearic acid-g-chitosan oligosaccharide micelle. Carbohydr Polym. 2011;83(4):1715–22.
47. Zhou H, Yu W, Guo X, Liu X, Li N, Zhang Y, *et al.* Synthesis and characterization of amphiphilic glycidol−chitosan−deoxycholic acid nanoparticles as a drug carrier for doxorubicin. Biomacromolecules. 2010;11(12):3480–6.
48. Jin Y-H, Hu H-Y, Qiao M-X, Zhu J, Qi J-W, Hu C-J, *et al.* pH-sensitive chitosan-derived nanoparticles as doxorubicin carriers for effective anti-tumor activity: preparation and in vitro evaluation. Colloids Surf B: Biointerfaces. 2012;94:184–91.
49. Lao SB, Zhang ZX, Xu HH, Jiang GB. Novel amphiphilic chitosan derivatives: synthesis, characterization and micellar solubilization of rotenone. Carbohydr Polym. 2010;82(4):1136–42.
50. Mekhail GM, Kamel AO, Awad GAS, Mortada ND. Anticancer effect of atorvastatin nanostructured polymeric micelles based on stearyl-grafted chitosan. Int J Biol Macromol. 2012;51:351–63.
51. Nam HY, Kwon SM, Chung H, Lee SY, Kwon SH, Jeon H, *et al.* Cellular uptake mechanism and intracellular fate of hydrophobically modified glycol chitosan nanoparticles. J Control Release. 2009;135(3):259–67.
52. Amiji MM. Pyrene fluorescence study of chitosan self-association in aqueous solution. Carbohydr Polym. 1995;26(3):211–3.
53. Kataoka K, Harada A, Nagasaki Y. Block copolymer micelles for drug delivery: design, characterization and biological significance. Adv Drug Deliv Rev. 2001;47(1):113–31.
54. Fan L, Li F, Zhang H, Wang Y, Cheng C, Li X, *et al.* Co-delivery of PDTC and doxorubicin by multifunctional micellar nanoparticles to achieve active targeted drug delivery and overcome multidrug resistance. Biomaterials. 2010;31(21):5634–42.